GPM Satellite Simulator over Ground Validation Sites

BY TOSHIHISA MATSUI, TAKAMICHI IGUCHI, XIAOWEN LI, MEI HAN, WEI-KUO TAO, WALTER PETERSEN, TRISTAN L'ECUYER, ROBERT MENEGHINI, WILLIAM OLSON, CHRISTIAN D. KUMMEROW, ARTHUR Y. HOU, MATHEW R. SCHWALLER, ERICH F. STOCKER, AND JOHN KWIATKOWSKI

THE GLOBAL PRECIPITATION MEASUREMENT (GPM) MISSION. The Global Precipitation Measurement (GPM) Core Observatory will be launched in February 2014. It will provide next-generation satellite rainfall measurement and better understanding of energy/water cycles in the weather and climate system after 15 years of successful operation of the Tropical Rainfall Measuring Mission (TRMM) satellite. In comparison with the TRMM satellite (±38° latitude), GPM will extend measurements to high latitudes (±65° latitude), where light precipitation and snowfall frequently occur over the continents. To meet accuracy requirements, the GPM Core satellite carries a combination of active and passive microwave sensors with improved capabilities to detect light rain and falling snow. The GPM Dual-frequency Precipitation Radar (DPR) provides radar observations at both Ku-band (13.6 GHz) (similar to TRMM Precipitation Radar), and Ka-band (35.5 GHz), where the latter includes a high-sensitivity mode designed for improved detection of light/frozen precipitation. The GPM Microwave Imager (GMI) includes 10–89-GHz channels (similar to the TRMM Microwave Imager) and 166–183 GHz channels. These sensor upgrades require more complex precipitation algorithms that harness multisensor and multifrequency satellite signals to estimate warm/cold/mixed-phase precipitation rate over various precipitation regimes.

Prior to the Core Observatory launch, the "day-one" GPM operational precipitation algorithms and their associated products must be tested using proxy data to demonstrate their validity.[1] Algorithm testing requires representative measurements of GPM-observable signals associated with geophysical parameters (e.g., precipitation rate). One approach is to use a combination of in situ microphysics profiles (point observation) and airborne remote-sensing data from field campaigns, but sampling deficiencies limit the broad applicability of this method. A different approach is to use a database constructed from a Cloud-System Resolving Model (CSRM),[2] and to generate synthetic data for testing. Prior to the TRMM satellite launch (1997), the Goddard Cumulus Ensemble model with bulk single-moment microphysics was widely used for such algorithm testing purposes (e.g., Meneghini and Kozu 1990).

AFFILIATIONS: MATSUI AND IGUCHI—NASA GSFC, Greenbelt, Maryland, and University of Maryland, College Park, College Park, Maryland; LI AND HAN—NASA GSFC, Greenbelt, Maryland, and Goddard Earth Sciences Technology and Research, Morgan State University, Baltimore, Maryland; TAO—University of Maryland, College Park, College Park, Maryland; PETERSEN—NASA GSFC, Wallops Flight Facility, Wallops Island, Virginia; L'ECUYER—University of Wisconsin—Madison, Madison, Wisconsin; MENEGHINI, HOU, SCHWALLER, AND STOCKER—NASA GSFC, Greenbelt, Maryland; OLSON—NASA GSFC, Greenbelt, Maryland, and University of Maryland, Baltimore County, Baltimore, Maryland; KUMMEROW—Colorado State University, Fort Collins, Colorado; KWIATKOWSKI—NASA GSFC, Greenbelt, Maryland, and George Mason University, Fairfax, Virginia
CORRESPONDING AUTHOR: Toshihisa Matsui, Code 612, NASA Goddard Space Flight Center, Greenbelt, MD 20771
E-mail: Toshihisa.Matsui-1@nasa.gov

DOI:10.1175/BAMS-D-12-00160.1

In final form 1 March 2013

[1] NASA's Earth science spaceflight missions now routinely generate geophysical data products within hours of the start of instrument operations, and public distribution usually occurs within about six months of launch.

[2] Nonhydrostatic mesoscale atmospheric model with horizontal grid spacings less than a few kilometers.

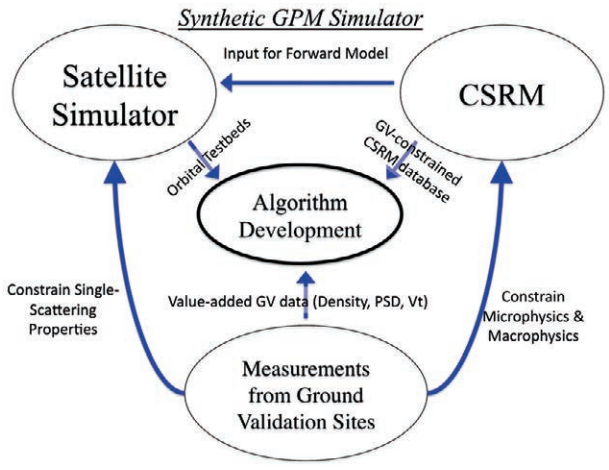

Fig. 1. Framework of the synthetic GPM simulator.

SYNTHETIC GPM SIMULATOR. During the GPM era, we developed the synthetic GPM simulator that integrates in situ observations, a CSRM, and satellite simulators to synergistically support development of the GPM precipitation algorithms. First, CSRM-simulated precipitation systems are evaluated and constrained by the in situ observations from various field campaigns. Second, GPM-observable signals are simulated from the CSRM-simulated geophysical parameters through the unified satellite simulators (Fig. 1). In this way, a bottom-up approach is taken to "upscale" in situ point measurements to CSRM scales (1 km), then to the sensor footprint scales (5–30 km), and finally to the satellite swath scales (125–1,500 km).

The GPM Ground Validation (GV) program. The GPM GV program recently conducted a series of field campaigns in mid- and high-latitude regions over Ontario, Canada [Canadian CloudSat/CALIPSO Validation Project (C3VP), the GPM Cold-season Precipitation Experiment (GCPEx)[3]], Helsinki, Finland [Light Precipitation Validation Experiment (LPVEx)], and Oklahoma, USA [Midlatitude Continental Convective Clouds Experiment (MC3E)], in order to study various types of precipitation processes. In addition to the main GV field campaigns, there were the NOAA Hydrometeorology Testbed (HMT) campaign over the Sierra Nevada Mountains and the DOE Tropical Warm Pool–International Cloud Experiment[4] (TWP-ICE) near Darwin, Australia (Table 1). The observations consisted of a suite of ground-based dual-polarimetric multifrequency radar, rain and snow gauges, disdrometers, and aircraft-based rainfall microphysics measurements (Table 2). Airborne remote sensors collected GMI/DPR-like measurements. Collectively, these ground and airborne datasets provide a set of GPM sensor-observable signals, coincident with ground-based and airborne observed rainfall rates, rain and snow size, and ice/snow bulk and particle shape characteristics. Not all of these parameters are directly retrieved via satellite remote sensing, but they are relevant to the formulation of a priori physical assumptions in algorithms. In each GV campaign, we have identified two unique "golden-day" cases that capture ideal precipitation systems with intensive observations from the deployed instruments (Table 1).

The Weather Research and Forecasting Model with Spectral Bin Microphysics (WRF-SBM). The WRF-SBM is one of the most advanced CSRM designed to support the GPM satellite mission. The WRF-SBM was developed from the Advanced Research WRF version 3.1.1 and coupled with the SBM originally developed for the Hebrew University Cloud Model. In comparison with the previous CSRM simulations used in previous satellite simulator studies, the WRF-SBM has a number of new features and innovations. First, the WRF core allows for heterogeneous surfaces with a terrain-following coordinate system, rather than a flat terrain common to idealized CSRMs. This enables various terrain-induced storm simulations, such as orographic precipitation or lake-effect storms. Second, the WRF core features multiple nested domains to downscale synoptic-scale analyses (50–100 km) to resolve storm-scale dynamics (1-km horizontal grid spacing and 60 vertical layers). Therefore, mesoscale and synoptic-scale propagating precipitation systems, such as midlatitude convective systems, frontal systems, and high-latitude snow systems, can be simulated in addition to tropical precipitation.

Third, and most importantly, the WRF-SBM features explicit size-bin-resolving cloud microphysics rather than the bulk microphysics used in the previous TRMM algorithm CSRM support. Cloud hydrometeors are categorized into liquid droplets, ice crystals (plate, column, dendrite), snow aggregates,

[3] GCPEx cases are not included in the first version of the orbital database due to its recent conclusion, but will be included in the second version of the orbital database.

[4] TWP-ICE cases are generated from the Goddard Cumulus Ensemble Model with Spectra-Bin Microphysics.

Table 1. Description of GPM Ground Validation (GV) sites and additional sites, locations, golden-day cases, and precipitation systems.

Site Name	Location	Date	Details of Precipitation Systems
C3VP (Canadian CloudSat/CALIPSO Validation Project)	Ontario, Canada	1/19/2007	Lake-effect snow breeze. Narrow and shallow snowband.
		1/21/2007	Large-scale homogeneous storm event.
LPVEx (Light Precipitation Validation Experiment)	Helsinki, Finland	9/21/2010	Large-scale mixed-phase stratiform rain with relatively high (~2400 m) altitude of melting band.
		10/20/2010	Large-scale mixed-phase stratiform rain with low (~1000 m) altitude of melting band.
MC3E (Midlatitude Continental Convective Clouds Experiment)	Oklahoma, USA	4/25/2011	Multicell MCS and shallow stratiform rain.
		5/20/2011	Severe convection and extensive stratiform rain.
TWP-ICE (Tropical Warm Pool-International Cloud Experiment)	Darwin Island, Australia	1/23/2006	Propagating organized tropical convection.
		2/05/2006	Isolated cumulus congestus.
HMT (Hydrometeorology Testbed)	California, USA	12/30/2005	Frontal orogenic mixed-phased rainfall (matured).
		12/31/2005	Frontal orogenic mixed-phased rainfall (decaying).

graupel, and hail in the SBM. The discrete particle size distributions (PSDs) of the hydrometeor classes are represented by 43 bins covering a large range of particle sizes, unlike the fixed-shape PSDs in bulk microphysics schemes. The melting and riming processes are also explicitly calculated for each snow aggregate size bin, allowing for a natural transition between hydrometeor species rather than the spontaneous conversion used in more common bulk microphysics formulations.

Because of its complexity, the WRF-SBM demands an order-of-magnitude greater computational resource than the WRF using a bulk microphysics scheme. We have conducted and stored several testbed cases with the WRF-SBM on the Pleiades supercomputer, operated by the NASA Advanced Supercomputing division in the NASA Ames Research Center. A 24-h WRF-SBM simulation generally requires ~5,000 processors and ~2 TB of storage for hourly output data. With such computational power, the WRF-SBM can provide more detailed microphysics (PSDs, effective density, melt fraction) information at higher resolution (1-km horizontal grid spacing) and over a larger area (~250,000 km^2) than the idealized CSRM used in the TRMM prelaunch era. The accuracy of the simulations with the bin microphysics scheme will be improved by incorporating various constraints derived from detailed GV observations.

GV-constrained WRF-SBM. The procedure to establish a GV-constrained WRF-SBM system includes a number of steps. First, a time series of simulated three-dimensional radar reflectivity of weather radar is computed from the WRF-SBM, and the instantaneous macrostructure of precipitation systems is evaluated by comparing the spatial and temporal variability of the simulated reflectivity to observations from the operational weather radar. During this evaluation step, the lateral and surface boundary forcing (analysis) or initial conditions of the WRF-SBM simulation are modified for forecast improvement.

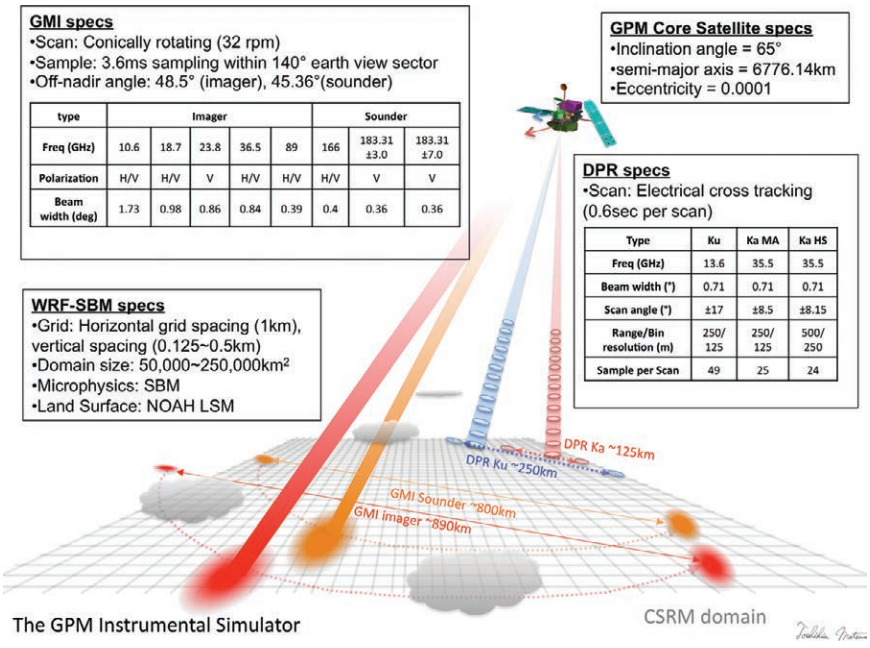

Fig. 2. Schematics of the GPM satellite simulator and the specifics of the GPM Core Observatory. Note that the swath widths vary slightly at different latitudes due to the Earth's oblateness.

Second, the statistical properties of the simulated radar echoes—such as the echo-top height and the maximum intensity in the column—are evaluated. These statistical parameters can be used to help validate the WRF-SBM-simulated microphysics profiles. Additional properties of the PSDs such as hydrometeor effective densities and terminal velocities are further evaluated against the aircraft- and ground-based in situ measurements (Table 2). The individual measurement specifications of the in situ instruments are implemented to compute instrument-equivalent parameters from the WRF-SBM through the guidance from GV scientists. This software module, the GV simulator, is a newly developed component in the Synthetic GPM Simulator [see examples in Iguchi et al. (2012a)].

Based upon results from the detailed microphysics evaluation, we modify microphysics process parameters, such as the number of background aerosols, ice nuclei, ice collision and coalescence rate, and amount of supercooled water, to name some, in order to bring the model fields into alignment with the observations [see more details in Iguchi et al. (2012a; 2012b)].

The GPM satellite simulator. The GPM satellite simulator translates the WRF-SBM-simulated geophysical parameters into the GPM-observable L1B [raw instrumental signals: microwave brightness temperature (*Tb*) for the GMI and equivalent radar reflectivity factor (*Zm*) for the DPR] signals in an orbital format (Fig. 2). The GPM satellite simulator has been built upon the existing multisensor satellite simulator, the Goddard Satellite Data Simulator Unit (G-SDSU), which is the spinoff version of the SDSU. The G-SDSU integrates several independent FORTRAN modules: the IO Module, the Optics Module, the Surface Module, the Radiative Transfer Modules, the Radar Module, and the recently developed Scan Module. This FORTRAN-based package of modules constitutes a comprehensive end-to-end GPM satellite simulator. Brief explanations of the most important modules are included here.

First, instantaneous fields of PSD bins, melting/riming fraction, atmospheric profile (temperature, pressure, humidity), and surface parameters (surface elevation, surface type, geolocation) are incorporated from the WRF-SBM simulation into the IO Module. Due to the enormous file size of the WRF-SBM, the G-SDSU decomposes the WRF-SBM domains into small subdomains for each CPU and its memory through Message Passing Interface processing.

Second, using the center location of the WRF-SBM domain, the Scan Module calculated satellite track and instrument-specific field-of view (FOV). The satellite track is estimated via the Keplerian orbit and Kozai's 1st-order perturbation theory. Then, orbit parameters and satellite sensor scanning system/geometry (GMI imager/sounder and DPR Ku/Ka bands) are used to calculate time progress of FOV geolocation, sensor incident angles, and antenna gain functions for each instrument sampling (Fig. 2).

Third, particle single-scattering properties are computed at each WRF-SBM grid point via Lorenz-Mie method in the Optics Module. Effective refractive indices are computed through the Maxwell-Garnett method that accounts for bin-by-bin particle effective density (riming fraction) and melting fraction. Single-particle single-scattering

Table 2. Description of measurements and instruments deployed at the GPM GV sites. These data are used to evaluate the WRF-SBM.

GV Measurements		
Instruments		**Measurable**
Ground	Weather Radar	Three-dimensional C-band radar image
	NASA Polarimetric (NPOL) radar	S-band radar image and polarimetric parameters
	Vertical Pointing S-, Ku, W-band radar	Times series of reflectivity and Doppler velocity profiles
	2 Dimensional Video Disdrometor (2DVD)	Particle shape information
		Terminal velocity
		Rain rate (volumetric rate for snowfall)
	Particle Size and Velocity (PARSIVEL) Disdrometer	Bulk particle size distributions (PSDs), number concentrations
		Spectrum bulk terminal velocity
		Rain rate (volumetric rate for snowfall)
	Geonor Bucket	Rain rate (melted rain rate for snowfall)
Aircraft	W-band cloud radar	W-band radar reflectivity and Doppler velocity
	The Compact Scanning Millimeter-wave Imaging Radiometer (CoSMIR), Advanced Microwave Precipitation Radiometer (AMPR)	GMI-like microwave brightness temperature
	High-Altitude Imaging Wind and Rain, Airborne Profiler (HIWRAP)	DPR-like Ka-Ku radar reflectivity and Doppler velocity profiles
	Particle Measuring Systems (PMS) 2D-C and 2D-P	Particle 2D images
		Bulk PSDs, number concentrations
	Counterflow Virtual Impactor (CVI), Nevzorov Hot Wire probe	Bulk water content (melted amount for solid particles)
	Rosemont Icing Probe (RICE)	Voltage signals for presence of supercooled liquid water

properties are integrated over the explicit PSD and over the various species to represent bulk single-scattering properties. The Surface Module predicts land- and ocean-surface emissivity. Land-surface emissivity is computed from the Tool to Estimate Land Surface Emissivities at Microwave Frequencies (TELSEM), while water-surface emissivity is a function of salinity, wind speed, and temperature.

For the GMI sensor, top-of-atmosphere microwave *Tb*s are computed via the two-stream model with Eddington's Second Approximation using bulk single-scattering properties along FOV-satellite

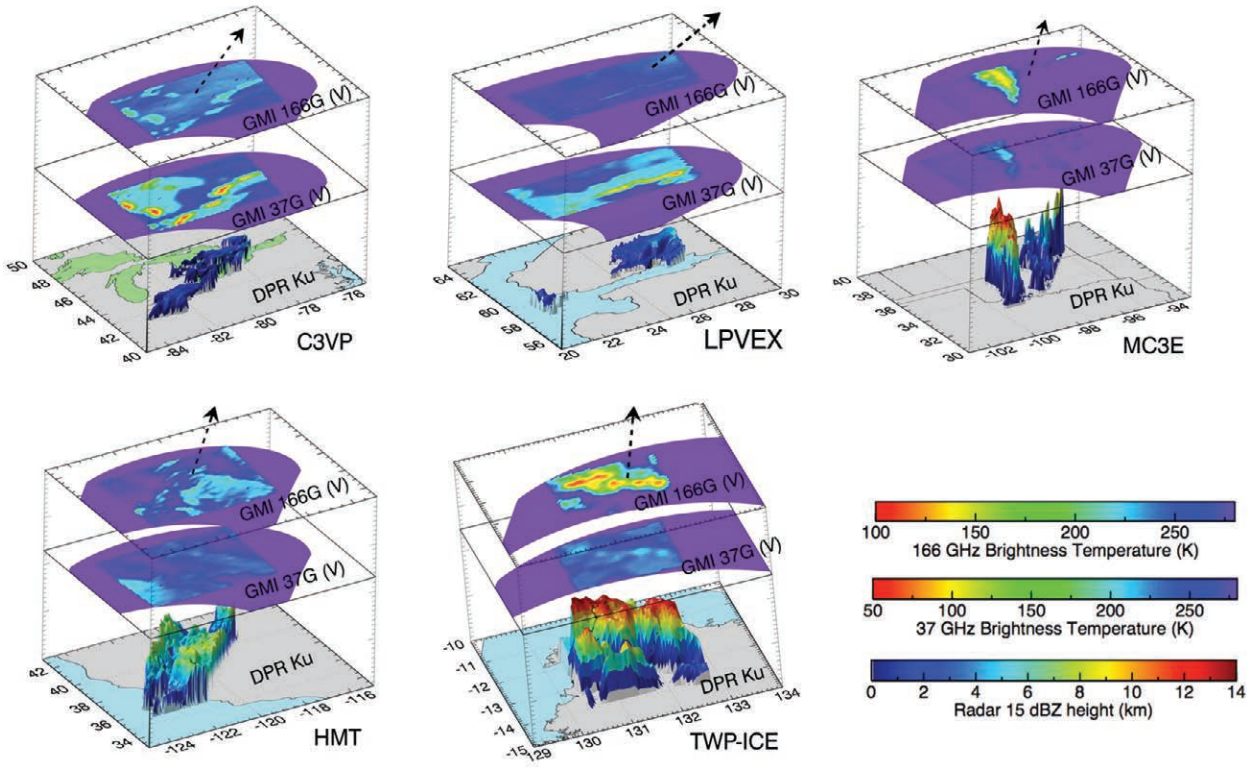

Fig. 3. Three-dimensional view of the simulated GPM orbital data over selected simulation scenes from C3VP, LPVEX, MC3E, HMT, and TWP-ICE. Color-shaded terrain represents 15 dBZ echo-top height of the DPR Ku band, and horizontal slices of color shades represent microwave brightness temperature of the GMI 37 and 166 GHz (V) channels.

slant paths in the Radiative Transfer Module. This slant-path approach mimics rigorous 3D microwave radiative transfer approach by using a 1D radiative transfer model. This module also considers the effect of terrain. Computed microwave *Tb*s are convolved over the antenna gain functions to represent measurements of brightness temperature over the footprint, called the Effective Field of View (EFOV). The EFOV describes the combined effects of the half-power beamwidth of the antenna gain and the radiometer sample integration period. GMI beam widths of the high- to low-frequency channels range from 0.4° (183 GHz) to 1.75° (10 GHz), corresponding to footprint sizes from 5 to 30 km, respectively.

The Radar Module calculates the attenuated and attenuation-corrected equivalent radar reflectivity factors (*Zm* and *Zt*, respectively) along the FOV-satellite path. Radar range (distance between radar returns and satellite positions) is estimated from the Scan Module. *Zm* and *Zt* are averaged over the individual pulse volumes using the Gaussian antenna gain pattern. In this process, terrain effects on radar sampling volume or area are used to account for the influence of surface-clutter effects in the cross-track scanning radar. At the radar range just above the surface, the total two-way path-integrated attenuation is estimated. Multiple scattering effects are not yet considered in the Radar Module. The vertical and horizontal sampling strategy in the Radar Module follows the GPM DPR algorithm.

Simulated Orbital GPM Testbed. The Simulated Orbital GPM Testbed consists of satellite orbital parameters, the GMI *Tb*s, and the DPR reflectivities. A total of 240 scenes of orbital data were generated from 10 GV cases for supporting GPM prelaunch algorithm development. Figure 3 displays simulated GMI *Tb* and DPR reflectivity from a selected scene of each site. The panel shows a diverse spectrum of simulated GPM satellite signals associated with different precipitation systems; however, the orbital database is limited over the WRF-SBM regional domain instead of an entire single orbit. The uniqueness of these simulated orbital data is the inclusion of the detailed retrieval-like

geophysical parameters derived from the WRF-SBM, such as rainfall rate, column water vapor, surface skin temperature, and moments of precipitation PSDs. These geophysical parameters are also processed with the same antenna convolution method as is done in the GMI and DPR modules. Thus, the satellite sensor–observable signals and algorithm-retrievable geophysical parameters are sampled in identical footprints within the same dataset, allowing algorithm scientists to quickly assess their retrieval algorithm products.

For convenience, the NASA Precipitation Processing System team converts the simulator output into the format adopted for the official GPM satellite products. The initial version (V1) of the synthetic orbital dataset is available at the ftp sites.[5] The official product can be readily visualized and checked by the new GPM-era free viewer THOR (the Tool for High-Resolution Observation Review).[6] The original WRF-SBM database is also available through the NASA GSFC Cloud Library.[7]

FUTURE DIRECTIONS. The GPM simulator utilizes improved observations, CSRMs, and satellite simulators compared to those used in the earlier TRMM prelaunch era. The comprehensive combination of detailed storm scenes with in situ data constraints and realistic forward models perhaps has not been previously achieved in other simulated datasets. Further improvement of the WRF-SBM simulations and the GPM satellite simulator is planned in the near future. Version 2 of the orbital database will feature a full upgrade of particle single scattering databases from the Lorenz-Mie method (spherical assumptions in particle shapes) to the Discrete-Dipole Approximation and T-matrix methods to account for the effects of complex structures of snow particles as observed from existing satellite measurements and polarimetric ground-based radar measurements. Microphysics of the WRF-SBM simulation will be further evaluated and improved upon the GV measurements. After the launch of the GPM Core satellite, the GPM satellite simulator will be a useful tool for radiance-based precipitation microphysics evaluation and assimilation methods (e.g., Matsui et al. 2009, Li et al. 2010, Han et al. 2013, Zupanski et al. 2011) using the GPM measurements.

[5] HDF version is available in ftp://trmmopen.gsfc.nasa.gov/pub/simulatedData, while NetCDF version is available in ftp://gpm.nsstc.nasa.gov/gpm_validation/related_projects/simulated_orbits.

[6] THOR is available at http://pps.gsfc.nasa.gov/tsdis/THOR/release.html.

[7] http://cloud.gsfc.nasa.gov/index.php?section=15

ACKNOWLEDGMENTS. The project is funded by the NASA Precipitation Measurement Mission (PMM) program (NNX11AR17G). The authors are grateful to Dr. R. Kakar at NASA HQ for his support of this research and also thank the NASA Advanced Supercomputing (NAS) Division in the NASA Ames Research Center. We also give thanks to many GV scientists, who provided useful datasets.

FOR FURTHER READING

Aires, F., C. Prigent, F. Bernardo, C. Jiménez, R. Saunders, and P. Brunel, 2011: A Tool to Estimate Land-Surface Emissivities at Microwave frequencies (TELSEM) for use in numerical weather prediction. *Quart. J. Roy. Meteor. Soc.*, **137**, 690–699.

Draine, B., and P. Flatau, 1994: Discrete-dipole approximation for scattering calculations. *J. Opt. Soc. Am. A Opt. Image Sci. Vis.*, **11**, 1491–1499.

Grasso, L., M. Sengupta, J. Dostalek, R. Brummer, and M. Demaria, 2008: Synthetic satellite imagery for current and future environmental satellites. *Int. J. Remote Sens.*, **29** , 4373–4384.

Han, M., S. A. Braun, T. Matsui, and C. R. Williams, 2013: Evaluation of cloud microphysics schemes in simulations of a winter storm using radar and radiometer measurements. *J. Geophys. Res. Atmos.*, **118**, 1401–1419, doi:10.1002/jgrd.50115.

Hou, A. Y., and Coauthors, 2013: The Global Precipitation Measurement (GPM) Mission. *Bull. Amer. Meteor. Soc.*, in press, doi:10.1175/BAMS-D-13-00164.1.

Iguchi, Takamichi, T. Matsui, J. J. Shi, W.-K. Tao, A. P. Khain, A. Hou, R. Cifelli, A. Heymsfield, and A. Tokay, 2012a: Numerical analysis using WRF-SBM for the cloud microphysical structures in the C3VP field campaign: Impacts of supercooled droplets and resultant riming on snow microphysics. J. *Geophys. Res.*, **117**, D23206, doi:10.1029/2012JD018101.

——, ——, A. Tokay, P. Kollias, and W.-K. Tao, 2012b: Two distinct modes seen in one-day rainfall event on the MC3E field campaign: Analyses of disdrometric data and WRF-SBM simulation. *Geophys. Res. Lett.*, **39**, L24805, doi:10.1029/2012GL053329.

Iguchi, Toshio, S. Seto, R. Meneghini, N. Yoshida, J. Awaka, and T. Kubota, 2010: GPM/DPR Level-2 Algorithm Theoretical Basis Document. [Available online at http://pmm.nasa.gov/sites/default/files/document_files/ATBD_GPM_DPR_n3_dec15.pdf.]

Khain, A., A. Pokrovsky, D. Rosenfeld, U. Blahak, and A. Ryzhkov, 2011: The role of CCN in precipitation and hail in a mid-latitude storm as seen in simulations using a spectral (bin) microphysics model in a 2D dynamic frame. Atmos. Res., **99**, 129–146.

Kidder, S. Q., 2002: Satellites: Orbits. *Encyclopedia of Atmospheric Sciences*, J. R. Holton, J. Pyle, and J. A. Curry, Eds., Academic Press, 2024–2038.

Kummerow, C., 1993: On the accuracy of the Eddington approximation for radiative transfer in the microwave frequencies. *J. Geophys. Res.*, **98**, 2757–2765.

L'Ecuyer, T., W. Petersen, and D. Moiseev, 2010: Light Precipitation Validation Experiment (LPVEx). [Available online at http://lpvex.atmos.colostate.edu/docs/lpvex_science_plan_June2010.pdf.]

Li, X., W.-K. Tao, T. Matsui, C. Liu, and H. Masunaga, 2010: Improving a spectral bin microphysical scheme using long-term TRMM satellite observations. *Quart. J. Roy. Meteor. Soc.*, **136**, 382–399.

Masunaga, H., and Coauthors, 2010: Satellite Data Simulator Unit: A multisensor, multispectral satellite simulator package. *Bull. Amer. Meteor. Soc.*, **91**, 1625–1632.

Matsui, T., X. Zeng, W.-K. Tao, H. Masunaga, W. Olson, and S. Lang, 2009: Evaluation of long-term cloud-resolving model simulations using satellite radiance observations and multifrequency satellite simulators. J. *Atmos. Oceanic Technol.*, **26**, 1261–1274.

Meneghini, R., and T. Kozu, 1990: *Spaceborne Weather Radar.* Artech House, 212 pp.

Mishchenko, M., L. Travis, and D. Mackowski, 1996: T-matrix computations of light scattering by non-spherical particles: A review. *J. Quant. Spectrosc. Radiat. Transf.*, **55**, 535–576.

Olson, W. S., P. Bauer, C. D. Kummerow, Y. Hong, and W.-K. Tao, 2001: A melting-layer model for passive/active microwave remote sensing applications. Part II: Simulation of TRMM observations. *J. Appl. Meteor.*, **40**, 1164–1179.

Simpson, J., R. F. Adler, and G. R. North, 1988: A proposed Tropical Rainfall Measuring Mission (TRMM) satellite. *Bull. Amer. Meteor. Soc.*, **69**, 278–295.

Wilheit, T. T., 1979: A model for the microwave emissivity of the ocean's surface as a function of wind speed. IEEE Trans. Geosci. Electron., **GE-17**, 244–249.

Zupanski, D., S. Q. Zhang, M. Zupanski, A. Y. Hou, and S. H. Cheung, 2011: A prototype WRF-based ensemble data assimilation system for dynamically downscaling satellite precipitation observations. *J. Hydrometeor.*, **12**, 118–134.